

Optimization of a collagen-targeted positron emission tomography probe for molecular imaging of pulmonary fibrosis.

Pauline Désogère¹, Luis F. Tapias², Tyson A. Rietz¹, Nicholas Rotile¹, Francesco Blasi¹, Helen Day¹, Justin Elliott², Bryan C. Fuchs³, Michael Lanuti², Peter Caravan¹.

¹Athinoula A. Martinos Center for Biomedical Imaging, Department of Radiology, Massachusetts General Hospital and Harvard Medical School, Charlestown, Massachusetts.

²Division of Thoracic Surgery, Massachusetts General Hospital and Harvard Medical School, Boston, Massachusetts.

³Division of Surgical Oncology, Massachusetts General Hospital and Harvard Medical School, Boston, Massachusetts.

Correspondence: Peter Caravan, PhD, Building 149, Room 2301, 13th Street, Charlestown, MA 02129, USA. Phone: 617-643-0193, FAX: 617-726-7422, Email: caravan@nmr.mgh.harvard.edu

First author: Pauline Désogère, PhD, Building 149, Room 6401, 13th Street, Charlestown, MA 02129, USA. Phone: 617-774-9905, FAX: 617-726-7422, Email: desogere@nmr.mgh.harvard.edu

Word count: 5440

Financial support: R01HL116315, R01HL131907 (National Heart and Lung and Blood Institute), DE-SC0008430 (Harvard/MGH Nuclear Medicine Training program), S10RR029495 (National Center for Research Resources), S10OD010650 (NIH, Office of the Director).

Short title: Collagen PET probe for fibrosis imaging

ABSTRACT

There is a large unmet need for a simple, accurate, non-invasive, quantitative and high resolution imaging modality to detect lung fibrosis at early stage and to monitor disease progression. Overexpression of collagen is a hallmark of organ fibrosis. Here, we describe the optimization of a collagen-targeted positron emission tomography (PET) probe for staging pulmonary fibrosis.

Methods

Six peptides were synthesized, conjugated to a copper chelator, and radiolabeled with copper-64. The collagen affinity of each probe was measured in a plate-based assay. The pharmacokinetics and metabolic stability of the probes were studied in healthy rats. The capacity of these probes to detect and stage pulmonary fibrosis in vivo was assessed in a mouse model of bleomycin-induced fibrosis using PET imaging.

Results

All probes exhibit affinities in the low micromolar range ($1.6 \mu\text{M} < K_d < 14.6 \mu\text{M}$) and have rapid blood clearance. The probes showed 2- to 8-fold greater uptake in the lungs of bleomycin-treated mice compared to sham treated mice, while the distribution in other organs was similar between bleomycin-treated and sham mice. Probe ^{64}Cu -CBP7 showed the highest uptake in fibrotic lungs and the highest target:background ratios. The superiority of ^{64}Cu -CBP7 was traced to a

much higher metabolic stability compared to the other probes. The specificity of ^{64}Cu -CBP7 for collagen was confirmed by comparison with a non-binding isomer.

Conclusion

^{64}Cu -CBP7 is a promising candidate for in vivo imaging of pulmonary fibrosis.

Key-words

Fibrosis, lung, type I collagen, copper-64, PET imaging.

INTRODUCTION

Pulmonary fibrosis is a disease of non-reversible scarring resulting in cough, hypoxemia, and in many cases death. In pulmonary fibrosis, normal, healthy lung is replaced by fibrotic tissue (1). Idiopathic pulmonary fibrosis has a dismal prognosis, with a median survival of only approximately 3 years after diagnosis, and the prognosis for certain other fibrotic lung disease is only marginally better. There is significant heterogeneity with respect to disease progression within pulmonary fibrosis, however, as some patients exhibit only slow declines in lung function, while others experience very rapidly progressive disease. There is a critical need for new methods of identifying fibrosis, staging disease, monitoring change in disease and characterizing disease activity.

Fibrosis, regardless of its cause or location, is characterized by excess deposition of collagens, primarily type I collagen, and other extracellular matrix proteins in the parenchyma (2). There are currently few molecular imaging approaches to assess fibrosis (3). We previously reported a 16 amino acid disulfide-bridged cyclic peptide that was identified via phage display to recognize type I human collagen. This peptide was functionalized with 3 gadolinium chelates to provide magnetic resonance signal enhancement and the resulting probe EP-3533 showed excellent ability to detect and stage disease in preclinical models of cardiac (4, 5), hepatic (6-8) and pulmonary fibrosis (9). Based on our positive MR findings with EP-3533, we sought to develop an analogous PET probe to quantify pulmonary fibrosis. PET is frequently used to characterize lung pathology. In the absence of lung architectural distortion, which may be absent

early in fibrotic lung diseases, fibrosis may not be able to be distinguished from alternative X-ray-attenuating processes, such as inflammation, by high resolution computed tomograph. By combining collagen-specific PET with high resolution computed tomography, however, it may be possible to determine whether specific opacities and patterns identified by high resolution computed tomography are produced by a fibrosing disease (10). In addition the development of PET molecular imaging probes offers a shorter and more economical path to clinical translation compared to MR probes.

MATERIAL AND METHODS

Additional information is reported in the supplemental material (available at <http://jnm.snmjournals.org>).

Synthesis, Radiochemistry and Affinity of CBPs

We synthesized a series of peptides and the corresponding 1,4,7-triazacyclononane-1-glutaric acid-4,7-acetate (NODAGA) conjugates and then reacted with $^{64}\text{CuCl}_2$. The synthetic route was analogous for each probe. All chemicals were purchased commercially and used without further purification. The 1,4,7-triazacyclononane (TACN) was purchased from Chematech (Dijon, France). The peptide precursors of CBP7 and CBP11 were custom-made by American Peptide. $^{64}\text{CuCl}_2$ was obtained from the University of Wisconsin. $(^t\text{Bu})_3\text{NODAGA-NHS}$ was synthesized in-house following a published procedure (11). All intermediates and final compounds were purified by high-performance liquid chromatography using a Phenomenex Luna C18 column (250 mm \times 21.2

mm × 5 μm) and a gradient of water/acetonitrile with 0.1% trifluoroacetic acid. All intermediates and final compounds characterized by liquid chromatography-mass spectrometry using a Phenomenex Kinetex C18 column (150 mm × 4.6 mm × 5 μm) and a gradient of water/acetonitrile with 0.1% formic acid (Supplemental Fig. 1; Supplemental Tables 1-2). Chemical purities of these compounds were greater than 97%.

Peptides on resin were synthesized by standard Fmoc chemistry using solid-phase peptide synthesis on a CEM microwave peptide synthesizer (Matthews, NC) on a 0.25 mmol scale. The peptides Pep(n) were cleaved with a cocktail comprising trifluoroacetic acid / methanesulfonic acid (70% in water) / triisopropylsilane / dodecanethiol, then precipitated in diethyl ether. Each Pep(n) were dissolved in a solution of dimethylsulfoxide / water (1/15, 16 mL) and the solution was adjusted to pH 5.5 with a 0.1 M solution of sodium hydroxide. The cyclization reactions were stirred at room temperature for 24 hours. The cyclized peptides cPep(n) were then coupled to tri-tert-butyl protected (tBu)₃NODAGA-NHS in dimethylformamide, at pH 6.5 in the presence of diisopropylethylamine to give (tBu)₃NODAGA-cPep(n) after 24 h. Deprotection of the tert-butyl groups with the cleavage cocktail described above resulted in the synthesis of NODAGA-cPep(n). NODAGA-cPep(n) were then isolated by precipitation in diethylether and purified. Reaction of NODAGA-cPep(n) with an excess of ^{nat}CuSO₄ in 10 mM sodium acetate buffer (pH=5.5) resulted in the synthesis of the nonradioactive surrogates CBPn (n=1, 3, 5, 6, 7, 11).

The general procedure for the radiolabeling of CBPn (n= 1, 3, 5, 6) was as follows: $^{64}\text{CuCl}_2$ (3.7–14.8 MBq, in 30 μL) was diluted with 90 μL of pH 5.1 ammonium acetate buffer (40 mM). A 10 μL aliquot of a 0.1 mM ligand solution (in sodium acetate buffer, pH 4.1) was added and the reaction mixture was heated at 60 °C for 15 min. For CBP7 and CBP11, $^{64}\text{CuCl}_2$ was diluted with 90 μL of pH 8.0 sodium citrate buffer (10 mM). A 10 μL aliquot of a 0.1 mM ligand solution (in HEPES pH 7.4) was added and the reaction mixture was stirred at room temperature for 5 min. After reaction the probe was purified with a Sep-Pak C18 cartridge. The radiochemical purities of the final solutions were $\geq 99\%$ as determined by radio-HPLC with a Phenomenex Luna C18 column (150 mm \times 4.6 mm \times 5 μm) using a gradient of water/acetonitrile with 0.1% trifluoroacetic acid (Supplemental Fig. 2). The pH of the final solutions was adjusted to 7.4 using phosphate buffer saline and the radiolabeled CBPn were diluted in sucrose (80 mM in water) before injection into animals.

Collagen binding isotherms were obtained by following a method previously reported (4).

Pharmacokinetics and Metabolic Stability

Pharmacokinetics and metabolic stability were obtained by following a method previously reported (12).

Animal Model and Probe Administration

All experiments were performed in accordance with National Institutes of Health Guidelines for the Care and Use of Laboratory Animals and with the ARRIVE guidelines (13), and were approved by the Institution's Animal Care and Use Committee at Massachusetts General Hospital. A total of 60 mice and 6 rats were used in this study. Pulmonary fibrosis was induced in 10-week-old male C57/BL6 mice (20-28 g, Charles River Laboratories, N=32) by transtracheal administration of bleomycin (2.5 U/kg) in 50 μ L of phosphate buffer saline under direct vision using a small cervical incision (14). Sham animals (N=28) received the analogous volume of vehicle (phosphate buffer saline). The mice were injected 13 to 14 days after bleomycin instillation by intra-femoral catheter with approximately 3.7 MBq in approximately 0.1 mL of the dose solution measured with a dose calibrator (CRC-25PET, Capintec).

Small Animal PET-CT Imaging and Analysis

Animals were placed in a small-animal PET/CT scanner (Triumph; TriFoil Imaging), equipped with inhalation anesthesia and heating pad. Each animal was anesthetized with isoflurane (4% for induction, 1-1.5% for maintenance in medical air). After placement of an in-dwelling catheter in the femoral vein for probe administration, mice were positioned in the PET-CT scanner and the probe was given as a bolus as the PET acquisition began. Mice were imaged continuously by PET for 120 minutes. A whole body CT was obtained either immediately before or immediately after the PET acquisition, the mice were then euthanized at 150 minutes post injection. Instrument calibration was performed with phantoms containing small known amounts of radioactivity. Isotropic (0.3

mm) CT images were acquired over 6 min with 512 projections with 3 frames per projection (exposure time per frame, ~200 msec; peak tube voltage, 70 kV; tube current, 177 mA). PET and CT images were reconstructed using the LabPET software (TriFoil Imaging) and the CT data were used to provide attenuation correction for the PET reconstructions. The PET data were reconstructed using a maximum-likelihood expectation-maximization (MLEM) algorithm run over 30 iterations to a voxel size of 0.5x0.5x0.6 mm³. For the pharmacokinetic analyses, the PET data were reconstructed in 1 min (first 10 frames), 3 min (next 10 frames), and 10 min (last 8-10 frames) intervals out to 120 min post injection. Reconstructed PET/CT data were quantitatively evaluated using AMIDE software package (15). For each PET scan, volumes of interest were drawn over major organs on decay-corrected whole body coronal images. The radioactivity concentration within organs was obtained from mean pixel values within the volume of interest and converted to counts per milliliter per minute and then divided by the injected dose (ID) to obtain an imaging volume of interest-derived percentage of the injected radioactive dose per cubic centimeter of tissue (%ID/cc).

Biodistribution Protocol

The lungs, blood, urine, heart, liver, left rectus femoris muscle, spleen, small intestine, kidneys, left femur bone were collected from all animals 150 min post probe injection. The tissues were weighed, and radioactivity in each tissue was measured on a gamma counter (Wizard2 Auto Gamma, PerkinElmer). Tracer distribution was presented as percent injected dose per gram (%ID/g) for all

organs. For the lungs, tracer was also presented as percent injected dose per lung (%ID/lung).

Histology and Quantification of Collagen

For histological purposes, one of the two lungs was inflated and fixed with 10% formalin, embedded in paraffin, cut into 5- μ m-thick sections and stained with either Hematoxylin and Eosin or Picrosirius Red with a counterstain of Fast Green. The remaining lung was hydrolyzed in a concentrated hydrochloric acid solution and the amount of hydroxyproline was quantified by HPLC after a two-step derivatization process (16).

Statistics

Data were expressed as mean \pm standard error of mean. Differences between groups were compared using the Student t test and analysis of variance, followed by the Tukey post hoc test. A *P* value of less than 0.05 was considered significant.

RESULTS

Synthesis, Radiochemistry and Affinity of CBPs

The general synthetic route for the probes is shown in Fig. 1. CBP1, CBP3, CBP5 and CBP6 were obtained by reaction of the ligands with $^{64}\text{CuCl}_2$ in yields of 99% in ammonium acetate buffer (pH = 5.1). For CBP7 and CBP11, considerable improvements in radiochemical yield were obtained when the

labeling was performed at pH 8 in sodium citrate (10 mM). The reactions were quantitative with a specific activity ranging from 6-18 GBq/ μ mol.

CBP1, CBP3, CBP5, CBP6 and CBP7 exhibited moderate affinity and non-saturable binding to type I collagen ranging from 1.6 μ M to 14.6 μ M (Supplemental Table 3). The low micromolar affinities displayed by these five new copper compounds are similar to the affinity of the parent ligand EP-3533 which was previously reported to be 1.8 μ M (17). CBP11 is the D-Cysteine analogue of CBP7 and has no affinity for collagen ($K_d > 100 \mu$ M).

Pharmacokinetics and Metabolism in Rats

The copper-64 blood clearance profile was very similar for all five probes (Supplemental Fig. 3) with elimination blood half-lives ranging from 18 to 23 min (Supplemental Table 4). Radio-HPLC analyses of rat serum post probe injection (15 and 60 min post injection) are shown in Fig. 2A. CBP1, CBP3, CBP5 and CBP6 undergo decomposition into less hydrophobic metabolites due to peptidase activity. Metabolism was extremely rapid for CBP1, CBP3 and CBP5 with less than 50% of intact probe detected in the blood at 15 min post injection (Supplemental Fig. 4A). CBP6 was still largely intact at 15 min post probe injection (percentage of intact probe >80 , (Supplemental Fig. 4B) and then further metabolized in the next 45 min. CBP7 was completely intact in the serum at 60 min post injection and in indeed highly stable over time: more than 80% of the circulating activity is intact probe at 120 min post probe injection (Supplemental Fig. 4C).

Small Animal PET-CT Imaging and Analysis of the 5 Collagen-Binding Probes in Mice with Pulmonary Fibrosis and in Control Animals

Analysis of fused PET-CT images clearly demonstrated a higher probe uptake in the lungs of the bleomycin-treated mice compared to sham mice (Fig. 2B) for CBP1, CBP3, CBP5, CBP6 and CBP7. In the bleomycin-treated mice, the lung activity was higher than the adjacent muscle or the heart. The lung:background (muscle) ratio was consistently higher in the bleomycin-treated mice compared to the controls for all probes, and ranged from 1.5- to 3- fold higher, with the greatest contrast seen with CBP7. For CBP7, the lung uptake was about 4-fold higher in bleomycin-treated mice compared to controls (0.95 ± 0.14 %ID/cc versus 0.24 ± 0.1 , $P < 0.0001$; Fig 2B; Supplemental Fig. 5). One-way analysis of variance between activity values in fibrotic tissues with the different probes revealed strong statistical differences. The signal in the lungs of fibrotic mice injected with CBP7 was significantly higher than the signal in the lungs of the fibrotic animals injected with CBP3 ($P = 0.0047$), CBP5 ($P = 0.0071$) and CBP6 ($P = 0.0009$). The uptake in the fibrotic lungs ranged from 1.4 to 7-fold higher in the animals that received CBP7 compared to animals that received the other probes ($P < 0.05$).

Biodistribution in Mice with Pulmonary Fibrosis and in Control Animals of the 5 Collagen-Binding Probes

After PET-CT imaging, each probe was further assessed *ex vivo* by directly sampling tissues of interest (Supplemental Tables 5-9). Each probe

showed greater lung uptake in bleomycin-treated mice (fibrotic) compared to sham mice, and this increased uptake in fibrotic lung ranged from 2- to 8-fold that of the sham (Fig. 2C). The difference was statistically higher for CBP7 (0.017 ± 0.003 vs 0.107 ± 0.022 , sham vs bleomycin-treated, $P < 0.0001$). Among the 5 probes, CBP7 showed the highest uptake in fibrotic lungs ($P < 0.05$); there was no significant difference in the normal lung uptake between probes.

Apart from the lungs, all the probes showed a similar non-target uptake in control and bleomycin-treated animals. Uptake in liver for CBP3, CBP5, CBP6 and CBP7 ($2 < \%ID/g < 4$) may be attributed to a transmetallation phenomenon by endogenous proteins. All the probes were excreted primarily through the kidneys. Similar to most peptide-based probes, we observed some retention in the kidneys. CBP7 exhibited the highest uptake in the kidneys, 2 to 8-fold higher compared to the other probes in both sham ($P < 0.0001$) and bleomycin-treated animals ($P < 0.0001$).

Histology

All of the bleomycin-treated mice had histopathological findings consistent with substantial pulmonary fibrosis, including excessive deposition of collagen in the extracellular matrix as shown by picrosirius red staining (Fig. 3A), while the sham animals showed no signs of pulmonary disease. These results demonstrated that the bleomycin model successfully induces pulmonary fibrosis in mice, accompanied by excessive deposition of collagen, including type I, in the extracellular matrix.

Collagen Quantification

Hydroxyproline is a quantitative biomarker of collagen (18). Comparing all mice, the hydroxyproline content was significantly higher in the lungs of the bleomycin-treated mice than in the lungs of the sham animals (Supplemental Fig. 6A). Ex-vivo analysis showed a strong correlation between the injected dose per lung and the hydroxyproline content for CBP3 ($r^2 = 0.62$, $P < 0.001$, Fig. 3B), CBP5 ($r^2 = 0.78$, $P < 0.01$, Fig. 3C), CBP6 ($r^2=0.83$, $P<0.001$, Fig. 3D) and CBP7 ($r^2 = 0.74$, $P < 0.0001$, Fig. 3E). For CBP1, the correlation between %ID/lung and hydroxyproline content was much weaker ($r^2 = 0.11$, Supplemental Fig. 6B).

Specificity of CBP7

To demonstrate the specificity of CBP7 binding to collagen, the isomer CBP11 was prepared. CBP11 differs from CBP7 only in the chirality of the cysteine residue at position X4 (D-Cys for CBP11). CBP11 was investigated in bleomycin-treated mice and controls. There was no difference in lung uptake between a bleomycin-treated animal and a sham injected with CBP11 (Fig. 4A). This was confirmed by quantification of the PET data (Fig. 4B) and the *ex vivo* lung uptake (Fig. 4C). The biodistribution of CBP11 was assessed in sham animals and bleomycin-treated animals at 2.5 h after injection, and compared to CBP7 (Fig. 5; Supplemental Table 10). CBP11 uptake was similar in fibrotic lungs and in control lungs and showed a similar non-target uptake in control and bleomycin-treated animals. CBP11 concentration in blood was similar to the one of CBP7 as may be expected for the isomers in both cohorts. There was a trend

toward slower blood clearance in the bleomycin treated mice compared to sham mice for both CBP7 and CBP11, presumably because of disease, however the increased uptake of CBP7 in the lungs of bleomycin-treated mice was much higher than could be accounted for by increased blood activity in the lungs. There was no statistically significant difference in CBP7 and CBP11 uptake in lung, kidney, spleen, heart and liver in sham animals. In fibrotic lungs, CBP7 uptake was 3-fold higher compared to CBP11 uptake ($P=0.0047$).

DISCUSSION

Herein, we present the synthesis and the evaluation of 5 collagen binding probes: CBP1, CBP3, CBP5, CBP6 and CBP7 for detecting pulmonary fibrosis in a murine model. We used a core peptide that has high affinity and specificity for collagen (4). We previously used the MR probe EP-3533 to demonstrate specific MR imaging of pulmonary collagen. However EP-3533 contains three gadolinium chelates to overcome the sensitivity limitations of magnetic resonance imaging. However for a PET probe, only one imaging reporter is required. We reviewed the structure-activity data reported in the patent covering EP-3533 and chose the peptides used in CBP1, CBP3, CBP5, CBP6 and CBP7. Each peptide contains 17 amino acids, of which 11 are conserved to maintain collagen affinity. The disulfide bond was also shown to be essential (4). Positions X5, X7, X14, X15 and X16 were varied. These peptides, derivatized with Gd-DTPA at the N-terminus were shown to have similar affinity to type I collagen (17). We replaced the thiourea-conjugated DTPA with the NODAGA chelator linked via an amide bond. CBP1 and CBP6 had the same overall charge but different lipophilic groups

at different positions. CBP3 possessed an additional negative charge due to the presence of aspartic acid. For CBP6, an arginine was used to introduce an additional positive charge. We reasoned that varying the polarity, charge and lipophilicity of the peptide would lead to differences in metabolic stability and off-target distribution when assessed *in vivo*. As a reference we synthesized CBP7, which has the same amino acid sequence as EP-3533 but with three NODAGA chelators instead of GdDTPA moieties.

We choose copper-64 to take advantage of the favorable nuclear characteristics of this radioisotope and its availability with high specific activity (19). In a practical sense, copper-64 is a convenient radioisotope for preclinical screening. The 12.7 hr half-life of copper-64 provides the flexibility to prepare doses for whole cohorts of mice in a single labeling. The long half-life of copper-64 is also suitable for peptide-based probes, which normally require flexible radiolabeling condition and longer circulation times to achieve optimal targeting and uptake (20). The NOTA family of chelators, can be easily labeled in mild conditions and the resulting complexes are resistant to transmetallation (12).

As expected from the previous structure activity relationship data, all the probes exhibited a low micromolar affinity for collagen. While CBP1, CBP3, and CBP7 showed comparable affinity to that of the established probe EP-3533, the collagen affinity of CBP5 and CBP6 was somewhat lower. Although all five probes displayed collagen affinity in the low micromolar range, their performance in the bleomycin mouse model of pulmonary fibrosis was diverse. The pharmacokinetic profile was very similar for all the probes in terms of blood

clearance of radioactivity, but the metabolic stability varied substantively from one probe to another with CBP7 being the most metabolically stable.

An unexpected finding in this work was that the peptide with 3 NODAGA chelators (CBP7) showed much higher uptake in fibrotic lung than the peptides with 1 NODAGA chelator. This is likely due to the greater in vivo metabolic stability associated with this probe. The three large hydrophilic chelators in CBP7 appear to block peptidase activity. CBP7 also contains an unnatural amino acid (4,4'-biphenylalanine) at the C-terminus, but we note that CBP3 also contained an unnatural amino acid (2-naphthylalanine) at its C-terminus but CBP3 was much less stable in vivo. In a different family of peptides we previously showed that conjugating a chelating group at both the C- and N-terminus of the peptide effectively blocked peptidase degradation (21). However CBP7 showed remarkably high metabolic stability despite the absence of a chelator at the C-terminus. CBP7 remained intact in the blood over time, which allows for greater accumulation in fibrotic tissues. CBP6 also showed good metabolic stability but this was offset by 6-fold lower collagen affinity as compared to CBP7. The high metabolic stability of CBP7 may also explain its higher kidney retention; the intact probe is likely retained by the kidneys, while metabolites in the form of the simple ^{64}Cu -NODAGA chelate are more likely cleared.

The goal of this work is to develop a PET imaging probe to enable early detection and staging of lung fibrosis. A successful probe must fulfill the following criteria (1) high uptake in the fibrotic lungs, (2) specificity for disease, (3) low retention in off-target organs and (4) high target-to-background ratios.

While it is difficult to optimize for all these parameters concurrently, the compounds synthesized in this small series could be ranked with respect to their desirability for further translation. CBP7 proved superior in this regard, as well as with respect to metabolic stability. CBP7 also correlates well ($r^2 = 0.83$, $P < 0.0001$) with lung hydroxyproline (total collagen) demonstrating the ability of the probe to stage disease.

The specificity of CBP7 was attested by comparison with a non-binding isomer (CBP11), wherein one of the cysteine moieties is changed from L-Cys in CBP7 to D-Cys in CBP11. This change in chirality resulted in a greater than 100-fold loss in collagen affinity for CBP11; however, the distribution in normal animals was similar for both probes. The probes only behaved differently in bleomycin-treated mice, with CBP7 highly accumulated in fibrotic lungs.

There has been increasing interest in molecular imaging of pulmonary fibrosis. Established probes like the somatostatin receptor targeted ^{68}Ga -DOTANOC (22) and ^{18}F -FDG (23) have been evaluated in IPF patients. However the specificity of these probes for IPF compared to other pulmonary pathologies, like non-specific interstitial pneumonia, is not clear. A cysteine-cathepsin-targeted dual optical/PET probe ^{68}Ga -BMV101 was used to monitor the contribution of inflammatory macrophages to fibrotic disease progression in a mouse model and in a small human cohort (24). Overexpression of $\alpha_v\beta_6$ integrin by alveolar epithelial cells plays a crucial role in the pathogenesis of pulmonary fibrosis (25), and an ^{111}In -labeled peptide specific to $\alpha_v\beta_6$ (A20FMDV2) was used to measure $\alpha_v\beta_6$ expression in bleomycin-treated mouse lungs by single-photon emission

computed tomography (26). An F-18 labeled version of the peptide A20FMDV2 (GSK) is now under investigation in a Phase 1 clinical trial (Clinicaltrials.gov Identifier: NCT02052297).

The direct imaging of collagen method reported here is complementary to these techniques. Importantly, the strong correlation of lung uptake of CBP7 with hydroxyproline content, indicates the ability of this probe to stage pulmonary fibrosis.

One limitation of this work was the high kidney retention of CBP7 (%ID/g > 60) in mice, although the uptake in rat kidneys was much lower (9.2 %ID/g). The 12.7 h half-life of copper-64 would result in a greater radiation exposure to the kidney. In this regard, using a radionuclide with a shorter half-life such gallium-68 (68 min) or fluorine-18 (110 min) may be preferred for translation to humans (27). Work in that direction is ongoing.

CONCLUSION

We synthesized and evaluated five new collagen-targeted PET probes in a murine model of pulmonary fibrosis. Our best probe CBP7 showed a fast blood clearance, a high stability with respect to metabolism, a high target-to-background ratio and is specific for collagen. CBP7 represents a promising candidate for clinical translation of pulmonary fibrosis imaging.

DISCLOSURE

This project is supported the National Heart and Lung and Blood Institute (NHLBI) R01HL116315, R01HL131907. PD was supported by the Harvard/MGH Nuclear Medicine Training program, funded by the US Dept. of Energy (DE-SC0008430). Instrumentation support from the National Center for Research Resources (S10RR029495) and the Office of Director (S10OD010650) is acknowledged. P.C. has equity in Collagen Medical, the company, which holds the patent rights to the peptides used in these probes. P.C. and P.D. are inventors on patent/patent application (WO 2015196208) submitted by Massachusetts General Hospital that covers all probes.

References

1. Vancheri C, Failla M, Crimi N, et al. Idiopathic pulmonary fibrosis: a disease with similarities and links to cancer biology. *Eur Resp J*. 2010;35:496-504.
2. Wynn TA, Ramalingam TR. Mechanisms of fibrosis: therapeutic translation for fibrotic disease. *Nat Med*. 2012;18:1028-1040.
3. Zhou Y, Chen H, Ambalavanan N, et al. Noninvasive Imaging of Experimental Lung Fibrosis. *Am J Respir Cell Mol Biol*. 2015;53:8-13.
4. Caravan P, Das B, Dumas S, et al. Collagen-targeted MRI contrast agent for molecular imaging of fibrosis. *Angew Chem Int Ed Engl*. 2007;46:8171-8173.
5. Helm PA, Caravan P, French BA, et al. Postinfarction myocardial scarring in mice: molecular MR imaging with use of a collagen-targeting contrast agent. *Radiology*. 2008;247:788-796.
6. Polasek M, Fuchs BC, Uppal R, et al. Molecular MR imaging of liver fibrosis: A feasibility study using rat and mouse models. *J Hepatol*. 2012;57:549-555.
7. Farrar CT, DePeralta DK, Day H, et al. 3D molecular MR imaging of liver fibrosis and response to rapamycin therapy in a bile duct ligation rat model. *J Hepatol*. 2015;63:689-696.
8. Zhu B, Wei L, Rotile N, et al. Combined magnetic resonance elastography and collagen molecular magnetic resonance imaging accurately stage liver fibrosis in a rat model. *Hepatology*. 2017;65:1015-1025.
9. Caravan P, Yang Y, Zachariah R, et al. Molecular magnetic resonance imaging of pulmonary fibrosis in mice. *Am J Respir Cell Mol Biol*. 2013;49:1120-1126.
10. Blodgett TM, Meltzer CC, Townsend DW. PET/CT: form and function. *Radiology*. 2007;242:360-385.

11. Levy SG, Jacques V, Zhou KL, et al. Development of a multigram asymmetric synthesis of 2-(R)-2-(4,7,10-tris tert-Butylcarboxymethyl-1,4,7,10-tetraazacyclododec-1-yl)-pentanedioic acid, 1-tert-butyl ester, (R)-tert-bu4-DOTAGA. *Org Process Res Dev.* 2009;13:535-542.
12. Blasi F, Oliveira BL, Rietz TA, et al. Effect of chelate type and radioisotope on the imaging efficacy of four fibrin-specific PET probes. *J Nucl Med.* 2014;1157-1163.
13. McGrath J, Drummond G, McLachlan E, et al. Guidelines for reporting experiments involving animals: the ARRIVE guidelines. *Br J Pharmacol.* 2010;160:1573-1576.
14. Moeller A, Ask K, Warburton D, et al. The bleomycin animal model: a useful tool to investigate treatment options for idiopathic pulmonary fibrosis? *Int J Biochem Cell Biol.* 2008;40:362-382.
15. Loening AM, Gambhir SS. AMIDE: a free software tool for multimodality medical image analysis. *Mol Imaging.* 2003;2:131-137.
16. Hutson PR, Crawford ME, Sorkness RL. Liquid chromatographic determination of hydroxyproline in tissue samples. *J Chromatogr B, Analyt Technol Biomed Life Sci.* 2003;791:427-430.
17. Abujoub A, Buckler DR, Caravan PD, et al. US patent 9,386,938, 2016.
18. Kumar Srivastava A. Hydroxyproline: a potential biochemical marker and its role in the pathogenesis of different diseases. *Curr Protein Pept Sci.* 2016;17:596-602.
19. Wadas TJ, Wong EH, Weisman GR, et al. Coordinating radiometals of copper, gallium, indium, yttrium, and zirconium for PET and SPECT imaging of disease. *Chem Rev.* 2010;110:2858-2902.
20. Fichna J, Janecka A. Synthesis of target-specific radiolabeled peptides for diagnostic imaging. *Bioconj Chem.* 2002;14:3-17.

21. Zhang Z, Kolodziej AF, Qi J, et al. Effect of peptide-chelate architecture on metabolic stability of peptide-based MRI contrast agents. *New J Chem.* 2010;2010:611-616.
22. Ambrosini V, Zompatori M, De Luca F, et al. ⁶⁸Ga-DOTANOC PET/CT allows somatostatin receptor imaging in idiopathic pulmonary fibrosis: preliminary results. *J Nucl Med.* 2010;51:1950-1955.
23. Groves AM, Win T, Sreaton NJ, et al. Idiopathic pulmonary fibrosis and diffuse parenchymal lung disease: implications from initial experience with ¹⁸F-FDG PET/CT. *J Nucl Med.* 2009;50:538-545.
24. Withana NP, Ma X, McGuire HM, et al. Non-invasive Imaging of Idiopathic Pulmonary Fibrosis Using Cathepsin Protease Probes. *Sci rep.* 2016;6:19755.
25. Munger JS, Huang X, Kawakatsu H, et al. A mechanism for regulating pulmonary inflammation and fibrosis: the integrin alpha(v)beta6 binds and activates latent TGFbeta. *Cell.* 1999;96:319-328.
26. John AE, Lockett JC, Tatler AL, et al. Preclinical SPECT/CT imaging of $\alpha\beta 6$ integrins for molecular stratification of idiopathic pulmonary fibrosis. *J Nucl Med.* 2013;54:2146-2152.
27. Désogère P, Tapias LF, Hariri LP, et al. Type I collagen-targeted PET probe for pulmonary fibrosis detection and staging in preclinical models. *Sci Transl Med.* 2017;9:eaaf4696.

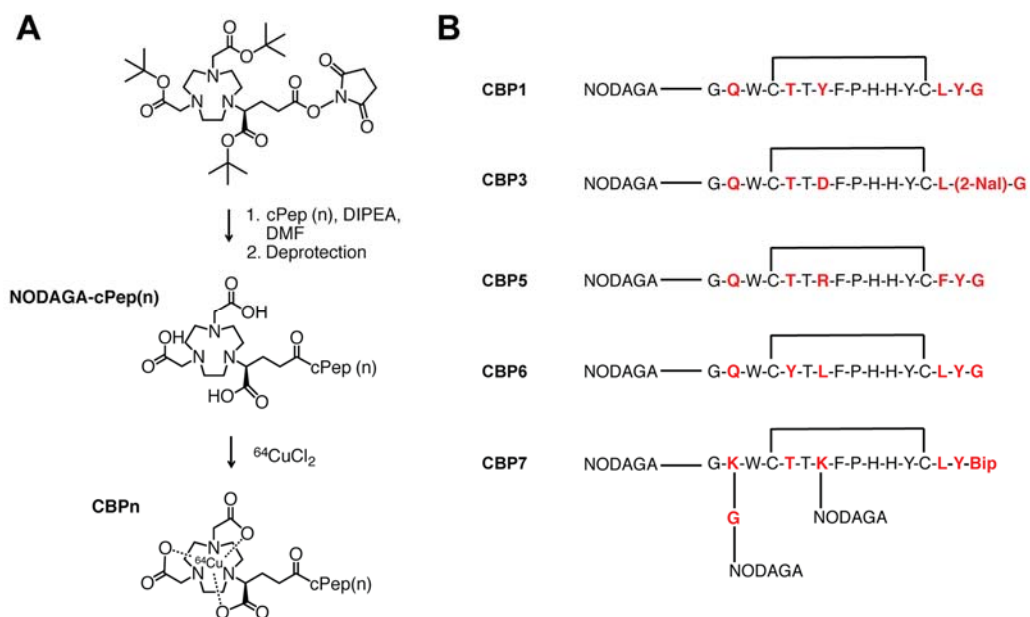


Figure 1. A. General protocol for synthesis of the collagen-binding probes (CBPs). **B.** Structures of the collagen-binding probes CBP1, CBP3, CBP5, CBP6 and CBP7. (Bip: 4,4'-biphenylalanine, 2-Nal: 2-naphthylalanine)

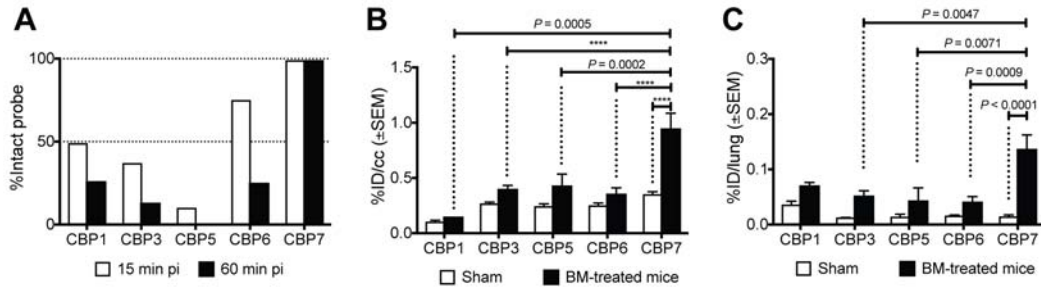


Figure 2. **A.** Metabolic stability of each probe estimated from HPLC analysis of serum samples in rat at 15 min and 60 min post probe injection. **B.** Ex-vivo lung uptake in sham and bleomycin (BM)-treated mice (2 weeks after bleomycin instillation) for CBP1, CBP3, CBP5, CBP6 and CBP7 at 150 min post probe injection (**** $P < 0.0001$). **C.** Mean lung PET activity values in sham and bleomycin-treated mice (2 weeks after bleomycin instillation) for CBP1, CBP3, CBP5, CBP6 and CBP7 (100-120 min after injection).

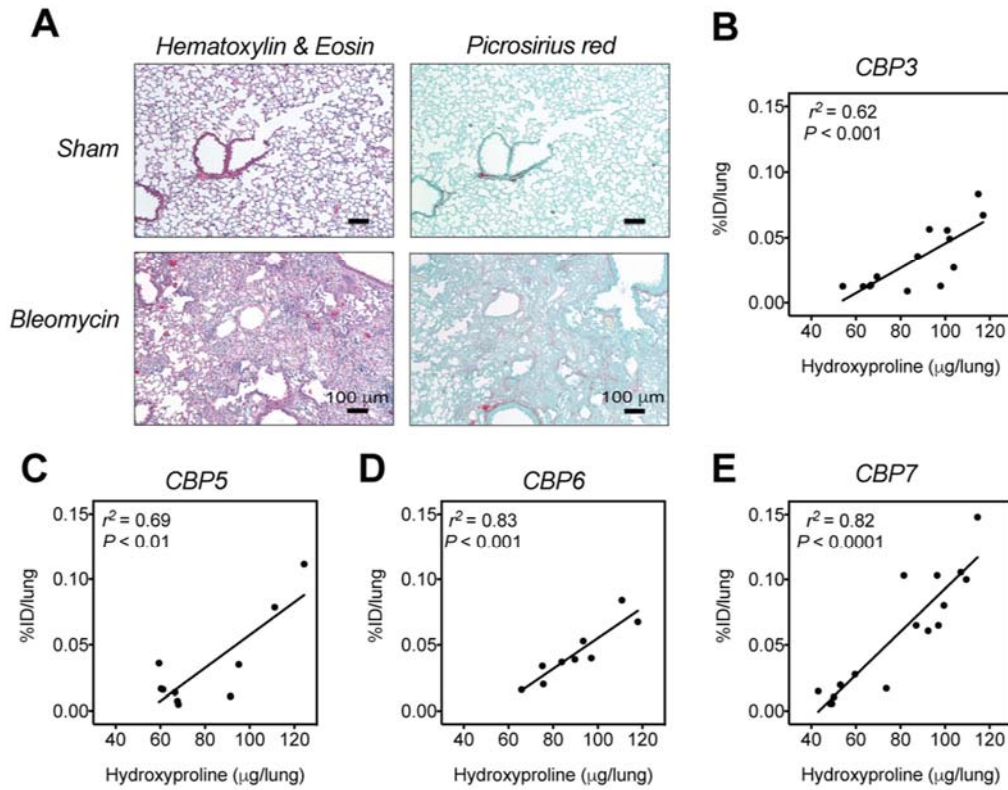


Figure 3. **A.** Representative images of lung tissue stained with hematoxylin and eosin and picrosirius red ($\times 10$, scale bar, 100 μm) for sham mice and for bleomycin-treated mice (2 week after bleomycin instillation). **B C. D. and E.** Correlation between hydroxyproline content as a measure of total lung collagen and %ID/lung in sham and bleomycin-treated mice, 2 weeks after instillation of bleomycin or vehicle and 150 min after probe injection.

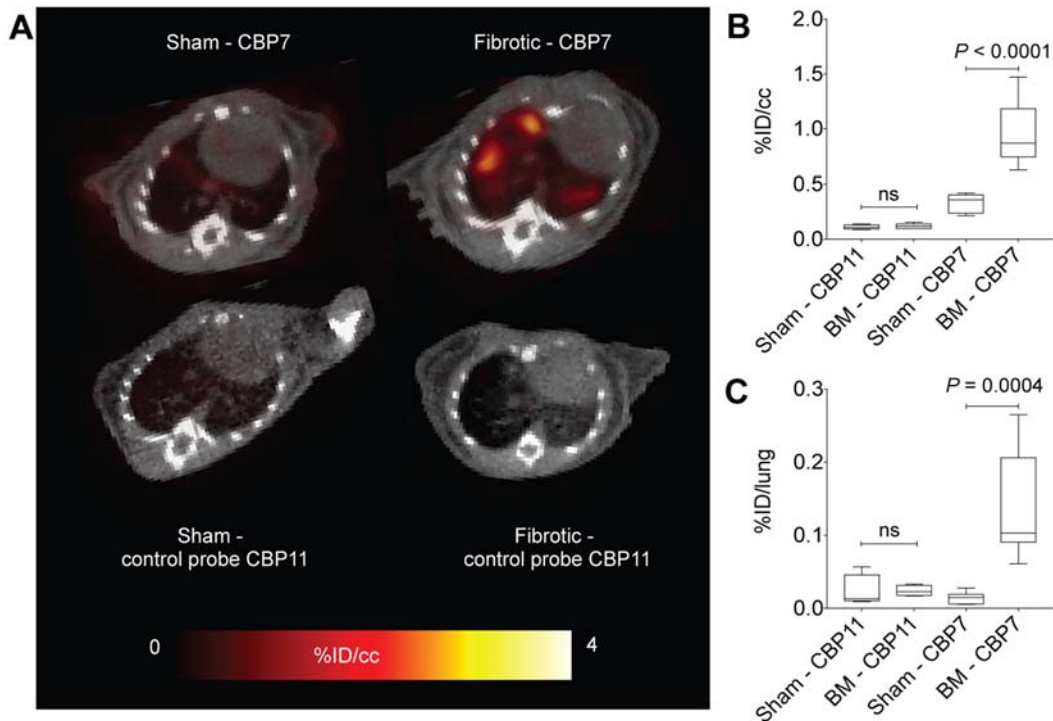


Figure 4. **A.** Representative fused PET-CT images (axial view) of sham and bleomycin (BM)-treated animals injected with CBP7 (top images) and CBP11 (bottom images). Color scale image shows PET image from integrated data 100-120 min post probe injection. **B.** Mean lung PET activity value in sham and bleomycin-treated mice for CBP7 and CBP11 from data 100-120 min after injection. **C.** Ex-vivo lung uptake in sham and bleomycin-treated mice at 150 min post CBP7 and CBP11 injection.

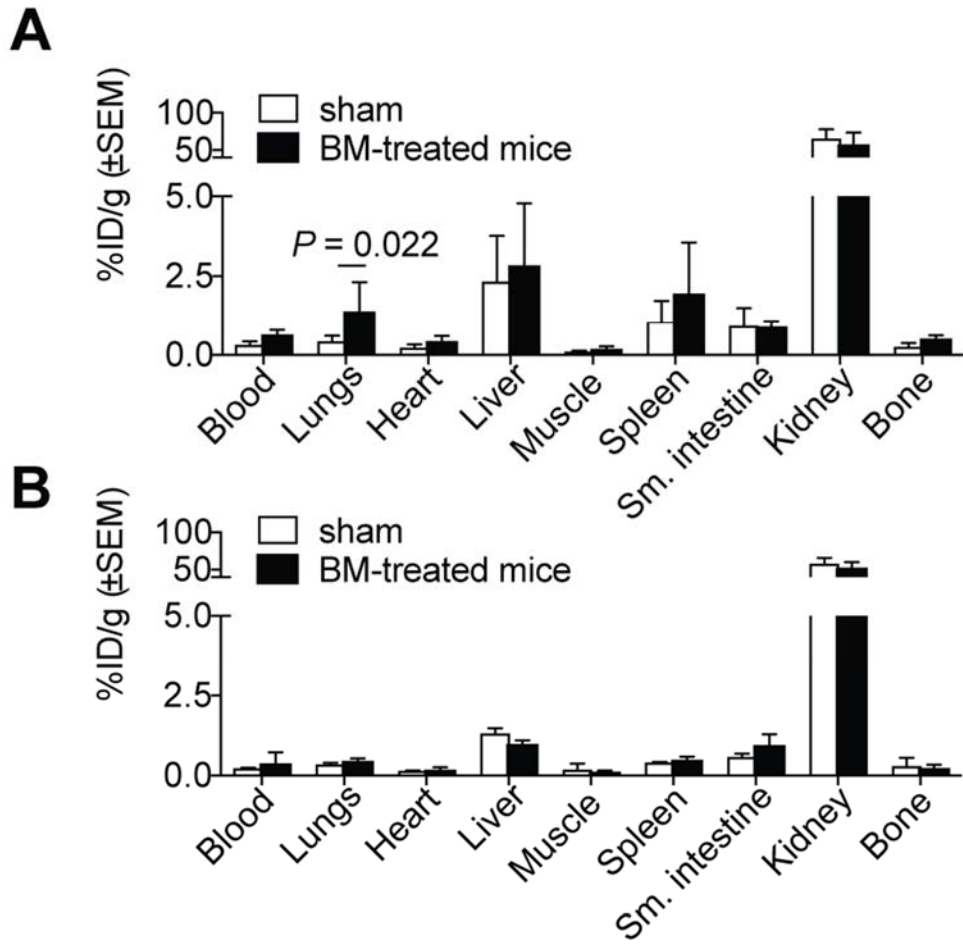


Figure 5. **A.** Biodistribution for CBP7 (n=7/group) and **B.** Biodistribution for CBP11 (n=4/group) in sham and bleomycin (BM)-treated mice, 120 min post probe injection.

Table 1. Lung to tissue ratio in bleomycin-treated mice at 150 min post injection.

Uncertainty is represented as standard error of mean.

	CBP1 (n=3)	CBP3 (n=6)	CBP5 (n=6)	CBP6 (n=6)	CBP7 (n=7)
blood	3.98 ± 0.96	4.59 ± 1.60	3.88 ± 2.26	2.43 ± 0.34	2.41 ± 0.85
heart	4.61 ± 0.75	5.00 ± 0.77	4.50 ± 1.97	3.46 ± 0.22	4.15 ± 1.49
liver	0.48 ± 0.13	0.27 ± 0.02	0.12 ± 0.07	0.23 ± 0.05	0.55 ± 0.07
muscle	5.23 ± 3.75	9.57 ± 2.89	14.26 ± 6.49	6.67 ± 1.39	11.91 ± 5.50
spleen	2.68 ± 0.56	0.91 ± 0.17	0.38 ± 0.24	0.78 ± 0.18	1.02 ± 0.22
small intestine	1.09 ± 0.16	1.08 ± 0.37	1.12 ± 0.75	0.64 ± 0.10	1.53 ± 0.34
kidney	0.03 ± 0.01	0.05 ± 0.01	0.02 ± 0.02	0.04 ± 0.01	0.02 ± 0.01
bone	3.56 ± 2.56	4.33 ± 1.07	2.00 ± 1.48	1.54 ± 0.19	2.62 ± 0.53

SUPPLEMENTAL DATA

Table of contents:

Figure 1. HPLC spectrum (UV=280 nm) of the precursors of CBP1, CBP3, CBP5, CBP6, CBP7 and CBP11

Figure 2. Radio-HPLC spectra of CBP1, CBP3, CBP5, CBP6, CBP7 and CBP11 showing purity.

Figure 3. Pharmacokinetic data showing blood clearance of the probes. Symbols indicate total copper-64 activity in the blood.

Figure 4. A. Representative radio-HPLC traces of intact CBP1 immediately isolated from serum (dashed line) and of serum collected 15 min post CBP1 injection (solid line), **B.** of intact CBP6 immediately isolated from serum (dashed line) and of serum collected 15 min post CBP6 injection (solid line), **C.** of intact CBP7 immediately isolated from serum (dashed line) and of serum collected 120 min post CBP7 injection (solid line).

Figure 5. Time-activity curves of lung and heart and lung and muscle from dynamic PET imaging in sham and BM-treated mice after CBP7 injection.

Figure 6. A. Hydroxyproline analysis of *ex vivo* harvested lung tissue from sham and bleomycin (BM)-treated animals (2 weeks after instillation of bleomycin). **B.** Correlation between hydroxyproline content as a measure of total lung collagen and %ID/lung in sham and bleomycin-treated mice, 2 weeks after instillation of bleomycin or vehicle and 150 min after CBP1 injection.

Table 1. LC-MS Species Identification of CBP1, CBP3, CBP5 and CBP6.

Table 2. LC-MS Species Identification of CBP7 and CBP11.

Table 3. K_d Values (μM) determined for collagen-binding probes through a rat tail collagen binding assay.

Table 4. Elimination half-life of the probes determined from blood samples in healthy rats.

Table 5. Tissue biodistribution of CBP1, 150 min post injection in sham and bleomycin-treated mice. Values are expressed in % ID/g \pm standard error of mean (SEM).

Table 6. Tissue biodistribution of CBP,3 150 min post injection in sham and bleomycin-treated mice. Values are expressed in % ID/g \pm SEM.

Table 7. Tissue biodistribution of CBP5 150 min post injection in sham and bleomycin-treated mice. Values are expressed in % ID/g \pm SEM.

Table 8. Tissue biodistribution of CBP6, 150 min post injection in sham and bleomycin-treated mice. Values are expressed in % ID/g \pm SEM.

Table 9. Tissue biodistribution of CBP7, 150 min post injection in sham and bleomycin-treated mice. Values are expressed in % ID/g \pm SEM.

Table 10. Tissue biodistribution of CBP11 150 min post injection in sham and bleomycin-treated mice. Values are expressed in % ID/g \pm SEM.

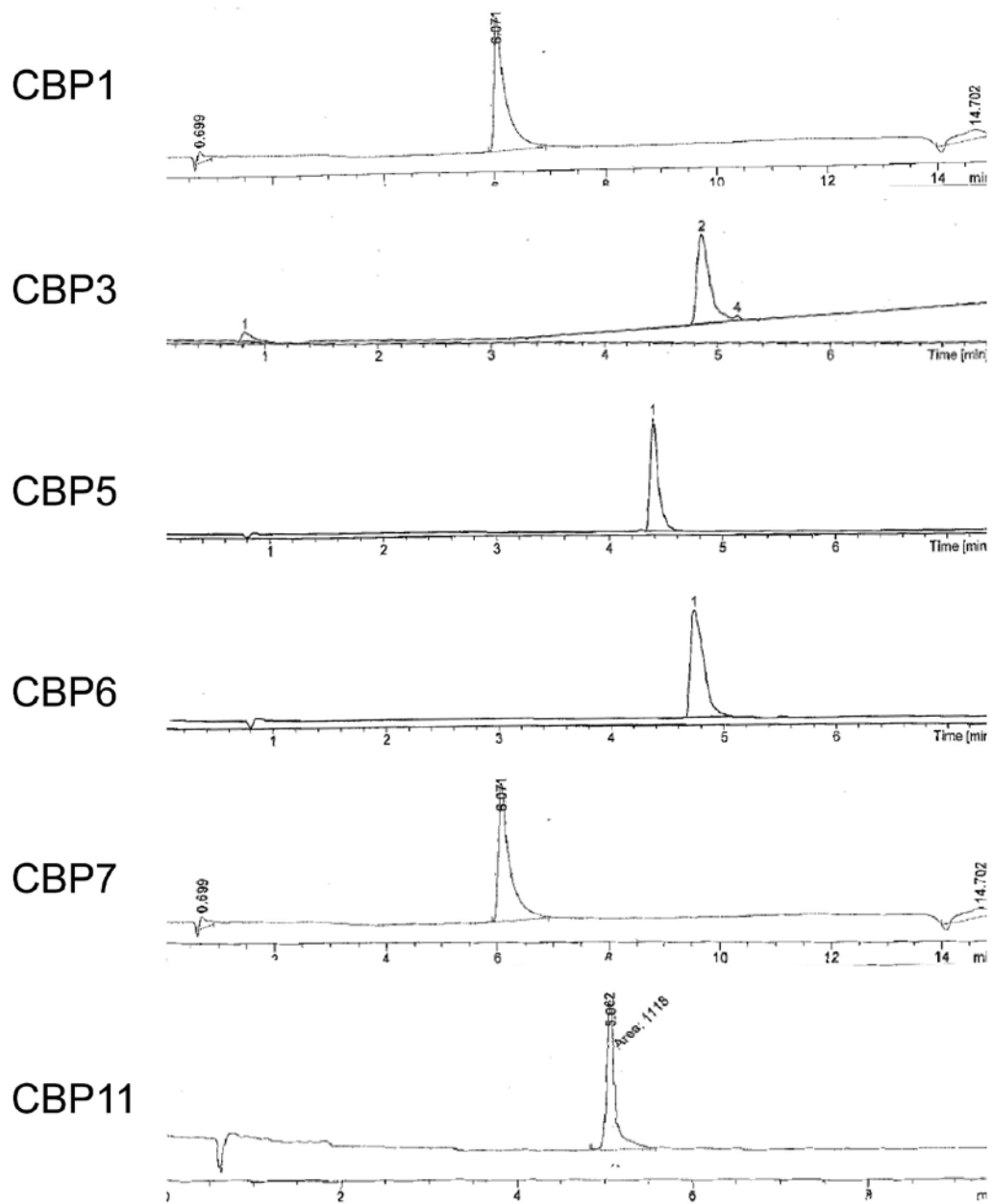


Figure 1. HPLC spectrum (UV=280 nm) of the precursors of CBP1, CBP3, CBP5, CBP6, CBP7 and CBP11

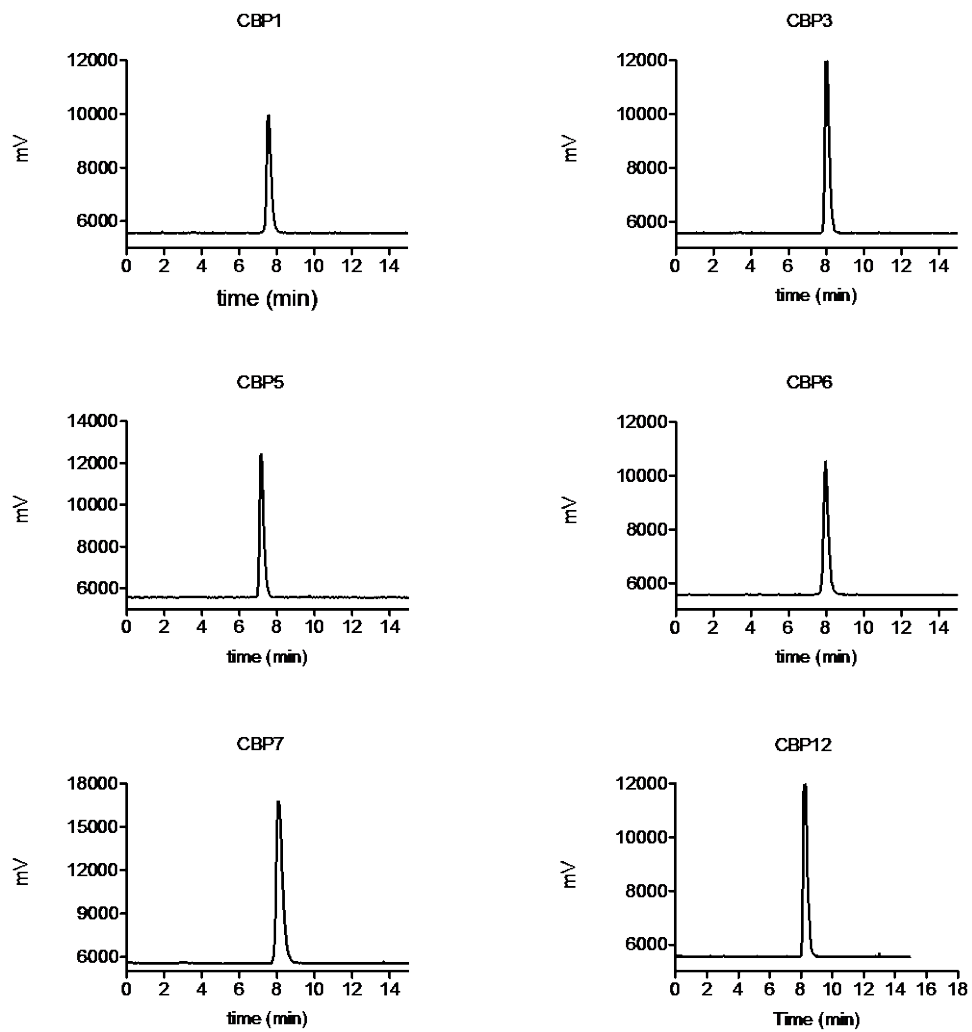


Figure 2. Radio-HPLC spectra of CBP1, CBP3, CBP5, CBP6, CBP7 and CBP11 showing purity.

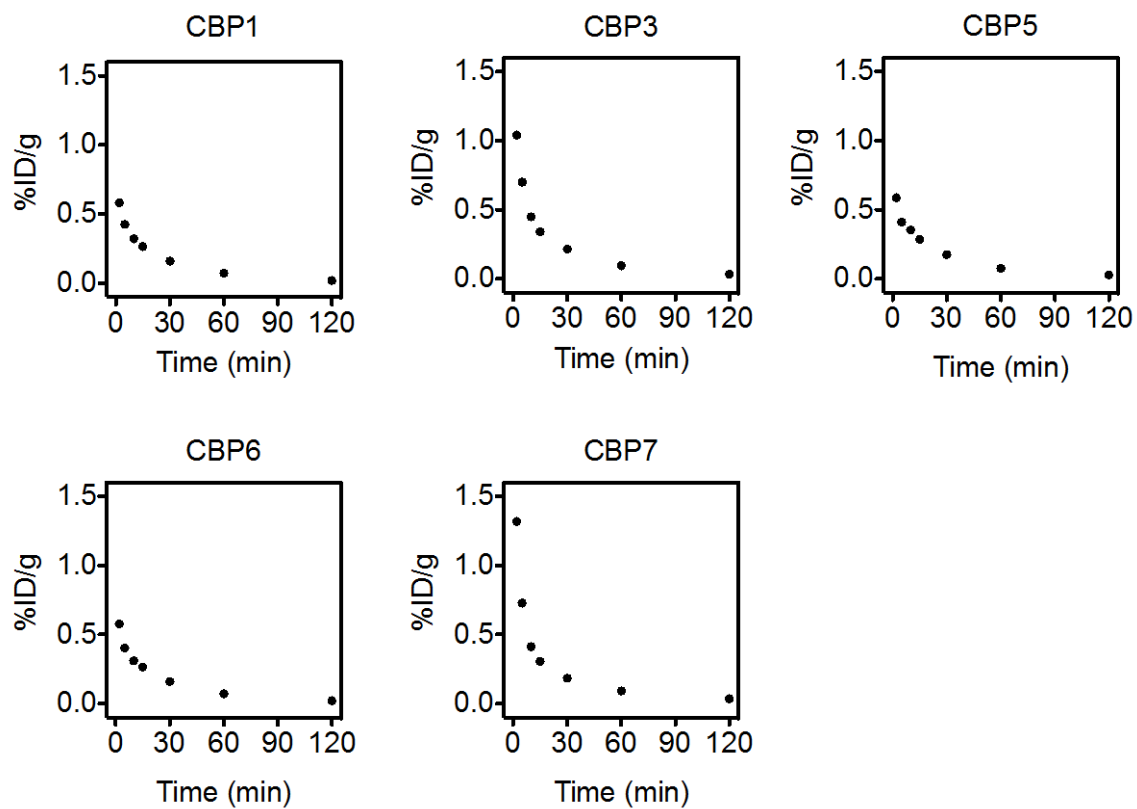


Figure 3. Pharmacokinetic data showing blood clearance of the probes. Symbols indicate total copper-64 activity in the blood.

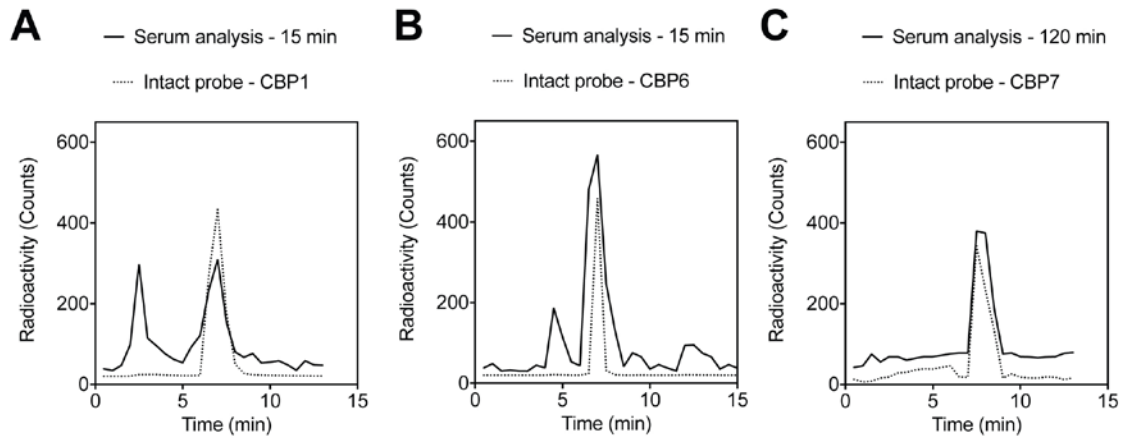
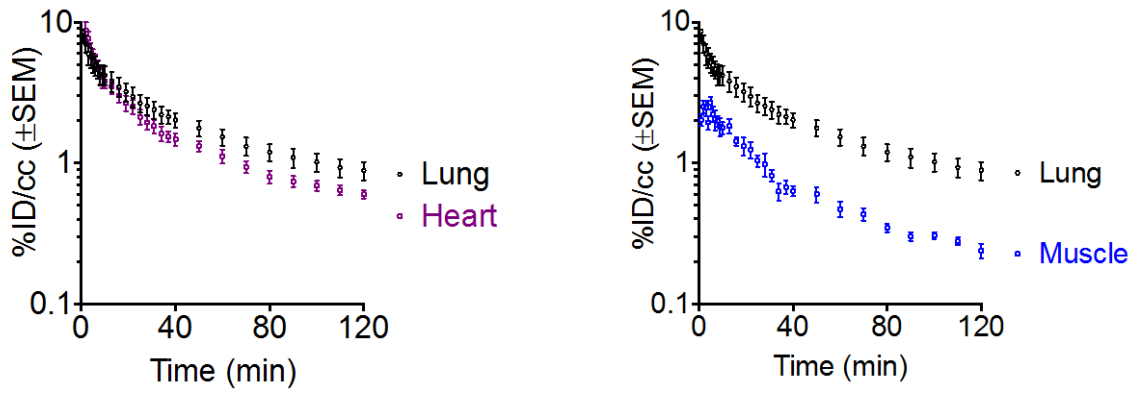


Figure 4. **A.** Representative radio-HPLC traces of intact CBP1 immediately isolated from serum (dashed line) and of serum collected 15 min post CBP1 injection (solid line), **B.** of intact CBP6 immediately isolated from serum (dashed line) and of serum collected 15 min post CBP6 injection (solid line), **C.** of intact CBP7 immediately isolated from serum (dashed line) and of serum collected 120 min post CBP7 injection (solid line).

BM - CBP7



Sham - CBP7

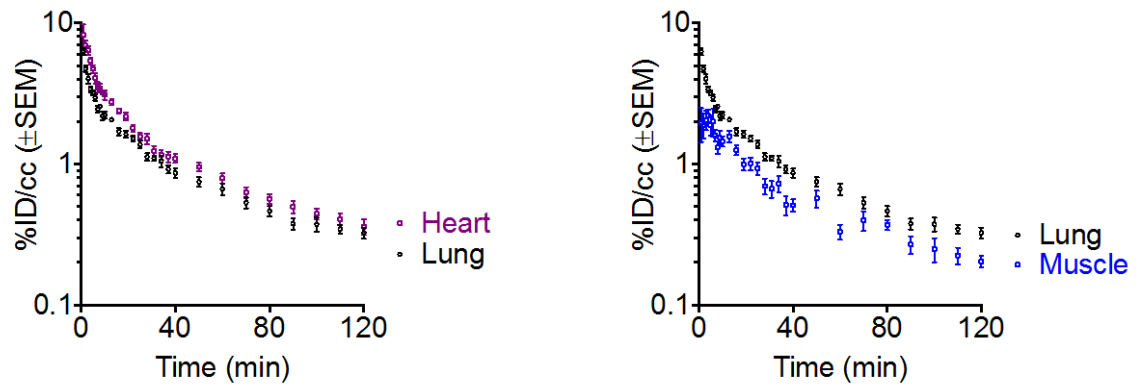


Figure 5. Time-activity curves of lung and heart and lung and muscle from dynamic PET imaging in sham and BM-treated mice after CBP7 injection.

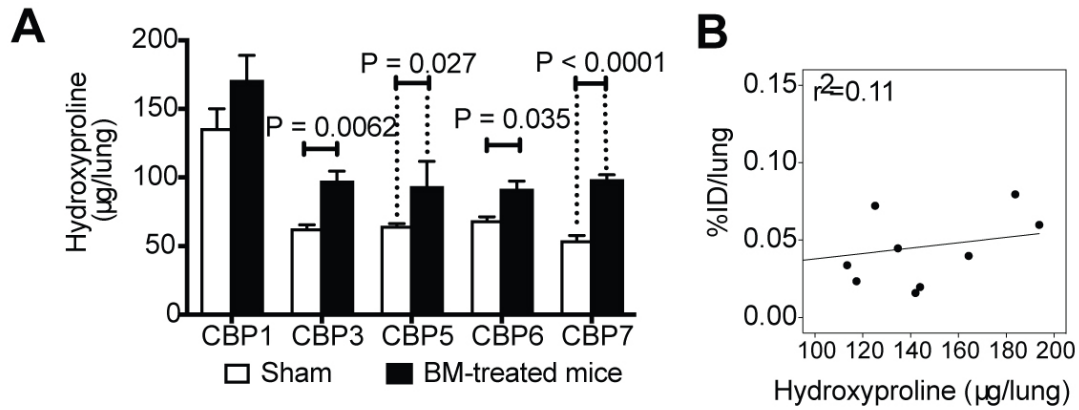


Figure 6. A. Hydroxyproline analysis of *ex vivo* harvested lung tissue from sham and bleomycin (BM)-treated animals (2 weeks after instillation of bleomycin). **B.** Correlation between hydroxyproline content as a measure of total lung collagen and %ID/lung in sham and bleomycin-treated mice, 2 weeks after instillation of bleomycin or vehicle and 150 min after CBP1 injection.

Table 1. LC-MS Species Identification of CBP1, CBP3, CBP5 and CBP6.

Specie	Chemical formula	Ion	
		m/2 calc	m/2 th
cPep(1)	C99H124N26O23S2	1056.1	1056.5
(tBu)3NODAGA-cPep(1)	C126H171N29O30S2	1319	1318
NODAGA-cPep(1)	C114H147N29O30S2	1234.9	1234.6
63/65Cu-NODAGA-cPep(1)	C114H145CuN29O30S2	1265.6	1265.5
cPep(3)	C98H122N26O23S2	1049.2	1049.2
(tBu)3NODAGA-cPep(3)	C125H169N29O30S2	1312	1311.3
NODAGA-cPep(3)	C113H145N29O30S2	1227.9	1227.1
63/65Cu-NODAGA-cPep(3)	C113H143CuN29O30S2	1258.6	1258.1
cPep(5)	C99H125N29O22S2	1069.7	1069.6
(tBu)3NODAGA-cPep(5)	C126H172N32O29S2	1332.5	1331.7
NODAGA-cPep(5)	C114H148N32O29S2	1248.4	1247.5
63/65Cu-NODAGA-cPep(5)	C114H146CuN32O29S2	1279.1	1279.1
cPep(6)	C101H128N26O22S2	1062.2	1061.6
(tBu)3NODAGA-cPep(6)	C128H175N29O29S2	1325	1325.3
NODAGA-cPep(6)	C116H151N29O29S2	1240.8	1239.7
63/65Cu-NODAGA-cPep(6)	C116H149CuN29O29S2	1271.5	1271.6

Table 2. LC-MS Species Identification of CBP7 and CBP11.

Specie	Chemical formula	Ion			
		m/3 calc	m/3 th	m/4 calc	m/4 th
NODAGA-cPep(7)	C157H213N37O43S2	ND*	ND	843.8	843.4
63/65Cu-NODAGA-cPep(7)	C157H207Cu3N37O43S2	1186	1186.2	ND	ND
NODAGA-cPep(11)	C157H213N37O43S2	ND	ND	843.8	843.5
63/65Cu-NODAGA-cPep(11)	C157H207Cu3N37O43S2	1186	1186.3	ND	ND

*ND (non detectable)

Table 3. K_d Values (μM) determined for collagen-binding probes through a rat tail collagen binding assay.

	K_d (μM)
CBP1	1.6 ± 1.1
CBP3	4.4 ± 1.0
CBP5	7.7 ± 5.2
CBP6	14.6 ± 5.8
CBP7	2.4 ± 1.5
CBP11	100

Table 4. Elimination half-life of the probes determined from blood samples in healthy rats.

	Half-life of the probe in rat (min)
CBP1	20.4
CBP3	23.4
CBP5	18.5
CBP6	20.2
CBP7	20.0
CBP11	21.3

Table 5. Tissue biodistribution of CBP1, 150 min post injection in sham and bleomycin-treated mice. Values are expressed in % ID/g \pm SEM.

CBP1	Sham (n=3)		bleomycin-treated mice(n=3)	
blood	0.09	\pm 0.02	0.10	\pm 0.02
lungs	0.38	\pm 0.06	0.59	\pm 0.20
heart	0.08	\pm 0.01	0.08	\pm 0.01
liver	0.71	\pm 0.01	1.07	\pm 0.28
muscle	0.12	\pm 0.06	0.26	\pm 0.16
spleen	0.14	\pm 0.01	0.31	\pm 0.18
sm. intestine	0.38	\pm 0.08	2.02	\pm 1.68
kidney	13.79	\pm 1.11	13.51	\pm 1.76
bone	0.14	\pm 0.03	0.30	\pm 0.17

Table 6. Tissue biodistribution of CBP3, 150 min post injection in sham and bleomycin-treated mice. Values are expressed in % ID/g \pm SEM.

CBP3	Sham (n=4)		bleomycin-treated mice (n=5)	
blood	0.17	\pm 0.02	0.49	\pm 0.31
lungs	0.36	\pm 0.01	0.70	\pm 0.08
heart	0.10	\pm 0.00	0.16	\pm 0.04
liver	2.01	\pm 0.07	2.57	\pm 0.24
muscle	0.05	\pm 0.00	0.14	\pm 0.04
spleen	0.21	\pm 0.02	0.97	\pm 0.24
sm. intestine	0.69	\pm 0.09	1.04	\pm 0.35
kidney	13.02	\pm 0.49	14.59	\pm 1.56
bone	0.13	\pm 0.01	0.29	\pm 0.13

Table 7. Tissue biodistribution of CBP5, 150 min post injection in sham and bleomycin-treated mice. Values are expressed in % ID/g \pm SEM.

CBP5	Sham (n=4)		bleomycin-treated mice (n=6)	
blood	0.11	\pm 0.02	0.12	\pm 0.03
lungs	0.30	\pm 0.06	0.45	\pm 0.13
heart	0.08	\pm 0.01	0.09	\pm 0.01
liver	2.63	\pm 0.15	3.84	\pm 0.77
muscle	0.47	\pm 0.41	0.03	\pm 0.01
spleen	0.81	\pm 0.42	1.59	\pm 0.55
sm. intestine	0.51	\pm 0.10	0.43	\pm 0.09
kidney	30.49	\pm 2.01	18.37	\pm 1.91
bone	0.70	\pm 0.34	0.49	\pm 0.24

Table 8. Tissue biodistribution of CBP6, 150 min post injection in sham and bleomycin-treated mice. Values are expressed in % ID/g \pm SEM.

CBP6	Sham (n=3)	bleomycin-treated mice (n=6)
blood	0.19 \pm 0.02	0.28 \pm 0.10
lungs	0.47 \pm 0.09	0.54 \pm 0.07
heart	0.15 \pm 0.02	0.16 \pm 0.02
liver	2.64 \pm 0.16	2.50 \pm 0.22
muscle	0.96 \pm 0.70	0.14 \pm 0.07
spleen	1.86 \pm 0.70	0.78 \pm 0.08
sm. intestine	1.17 \pm 0.20	0.94 \pm 0.16
kidney	21.07 \pm 4.04	14.01 \pm 0.73
bone	0.89 \pm 0.63	0.37 \pm 0.05

Table 9. Biodistribution in sham and bleomycin-treated mice at 150 min post injection) for CBP7. Uncertainty is represented as the as SEM.

CBP7	Sham (n=7)		bleomycin-treated mice (n=7)	
blood	0.31	± 0.04	0.63	± 0.06
lungs	0.42	± 0.07	1.37	± 0.36
heart	0.22	± 0.04	0.41	± 0.07
liver	2.32	± 0.54	2.82	± 0.74
muscle	0.09	± 0.02	0.18	± 0.03
spleen	1.06	± 0.25	1.94	± 0.61
sm. intestine	0.91	± 0.22	0.88	± 0.08
kidney	65.18	± 4.91	56.89	± 6.40
bone	0.25	± 0.05	0.50	± 0.04

Table 10. Biodistribution in sham and bleomycin-treated mice at 150 min post injection for CBP11. Uncertainty is represented as the as SEM.

CBP11	Sham (n=4)			bleomycin-treated mice(n=4)		
blood	0.22	±	0.02	0.37	±	0.18
lungs	0.34	±	0.03	0.44	±	0.05
heart	0.14	±	0.01	0.17	±	0.04
liver	1.30	±	0.09	0.95	±	0.07
muscle	0.18	±	0.10	0.10	±	0.03
spleen	0.41	±	0.01	0.48	±	0.06
sm. intestine	0.58	±	0.06	0.93	±	0.18
kidney	57.68	±	4.20	51.73	±	4.20
bone	0.29	±	0.14	0.22	±	0.06